Magnetization reversal in a (110)-oriented epitaxial $ErFe_2/DyFe_2$ Laves-phase superlattice

H. Fritzsche,* M. Saoudi, Z. Yamani, and W. J. L. Buyers
Canadian Neutron Beam Centre, Chalk River Laboratories, National Research Council Canada, Building 459, Chalk River, Ontario, Canada K0J 1J0

R. A. Cowley and R. C. C. Ward
Oxford Physics, Clarendon Laboratory, Parks Road, Oxford OX1 3PU, United Kingdom
(Received 14 August 2007; revised manuscript received 19 November 2007; published 20 February 2008)

The magnetization reversal of a Laves-phase superlattice has been measured by using unpolarized neutron diffraction and polarized neutron reflectometry. The superlattice (6 nm $ErFe_2$/6 nm $DyFe_2)_{40}$ consisted of two hard magnetic materials and was grown by molecular beam epitaxy with the [110] axis along the growth direction. The sample was mounted in a cryomagnet with a vertical field which was aligned along the $[1\bar{1}0]$ direction. The results of the diffraction experiment showed that during the magnetization reversal, the net magnetization reverses through the [221] direction close to the growth axis. The polarized neutron reflectivity confirmed this result and enabled the net layer magnetizations to be measured throughout the reversal. The results showed that both magnetizations were similar, but that the magnetization of the $DyFe_2$ reversed over a smaller range of applied fields.

DOI: 10.1103/PhysRevB.77.054423 PACS number(s): 75.60.Jk, 61.05.fj, 61.05.fm, 75.70.−i

I. INTRODUCTION

The need for magnetic materials for hard magnets, magnetic sensors, and magnetic recording materials requires the ability to control and tune the exchange forces and the magnetic anisotropy to produce useful materials. The magnetic rare earths are attractive materials because of their large moments, variable crystalline anisotropy, and differing exchange constants. However, with the exception of gadolinium, the pure metals have magnetic transition temperatures well below room temperature. In contrast, useful devices require the transition temperature to be above room temperature and this can be achieved by using the cubic Laves phase, $REFe_2$ compounds which are almost all ferromagnets with the anisotropy controlled by the rare earth (RE) and the strong exchange interaction supplied by the Fe.[1–3] In recent years, it has become possible to grow thin films and superlattices of these materials using conventional molecular beam epitaxy (MBE) techniques and $DyFe_2/YFe_2$ superlattices are the most studied system.[4–8] $DyFe_2$ is a hard magnetic material, whereas the YFe_2 is a soft ferromagnet with very little anisotropy. When a magnetic field is applied to the superlattices, they can exhibit an exchange spring behavior in which the magnetic moments in the $DyFe_2$ are pinned by the anisotropy, while the magnetic moments in the YFe_2 are rotated by the applied field toward the direction of the applied field. In the absence of an applied magnetic field, YFe_2 and $DyFe_2$ have magnetic moments that are oppositely aligned. If the lengths of the superlattice repeat are carefully chosen and a field is applied, then the system may also exhibit a spin-flop phase depending on the thickness of the two layers.[4–8]

In this paper, we study the behavior of a different superlattice consisting of two hard magnetic materials $ErFe_2$ and $DyFe_2$, which have differing easy axes for the magnetization. In the cubic bulk materials, the easy direction for the $ErFe_2$ magnetic moments is along the ⟨111⟩ directions, while for the $DyFe_2$, it is the ⟨100⟩ directions.[1] The superlattice is, however, not exactly cubic, and the strain results in a magnetoelastic anisotropy favoring the [110] growth direction for the $ErFe_2$ moments and a direction perpendicular to the growth direction for the $DyFe_2$ moments as determined from single thin films.[9,10] These layers are then coupled by the strong Fe-Fe exchange interaction so that we have a system with competing anisotropies and large exchange interactions.[3] The Fe-Fe exchange interaction for $ErFe_2$ and $DyFe_2$ is about 100 T, whereas the rare-earth–Fe interaction is about 20 T. We shall study the anisotropy of this system at low temperature and the way in which the magnetization reverses when a magnetic field is applied.

II. EXPERIMENTAL TECHNIQUES

The sample was grown at the MBE facility in the Clarendon Laboratory, Oxford. A sapphire substrate with a $(11\bar{2}0)$ orientation was cleaned, and 100 nm niobium was deposited as a chemical buffer layer, followed by a 2 nm iron seed.[7] The multilayer was then grown by codeposition of the elementary fluxes with a layer thickness of 6 nm for each layer, repeating the ($ErFe_2/DyFe_2$) sequence 40 times. Finally, the superlattice was covered with a 10 nm thick Y layer as a protection against oxidation. Both layers, $DyFe_2$ and $ErFe_2$, grew epitaxially with one another with [110] as the growth direction. These $REFe_2$ systems form the so-called Laves-phase structure (C15), with the RE atoms forming a diamond lattice and the Fe atoms forming tetrahedra around the RE atoms.[7]

With the C5 triple axis spectrometer at the neutron research reactor NRU in Chalk River, we performed unpolarized large angle neutron diffraction as well as grazing incidence polarized neutron reflectometry (PNR) experiments. For the unpolarized setup, we used a focusing pyrolytic graphite (PG) monochromator and a flat PG analyzer at a neutron wavelength of $\lambda = 0.237$ nm, whereas a Cu_2MnAl Heusler crystal was used for the polarized setup, also at $\lambda = 0.237$ nm. For both cases, a PG filter[11] reduced the higher

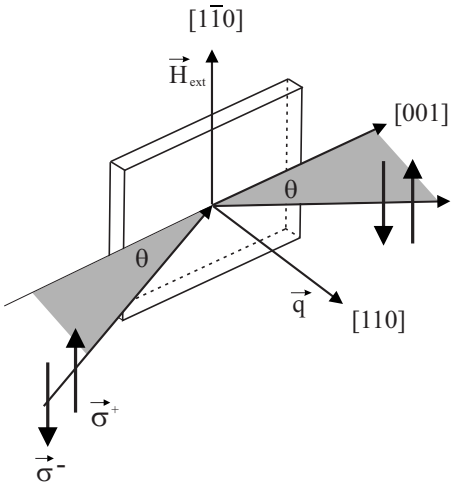

FIG. 1. Sample and scattering geometry used for the PNR as well as for the diffraction reversal experiments, with the external field H_{ext} along the in-plane [1$\bar{1}$0] direction and the scattering vector **q** parallel to the [110] out-of-plane direction. The spins $\boldsymbol{\sigma}^+$ of up-neutrons and $\boldsymbol{\sigma}^-$ of down-neutrons are parallel or antiparallel to the external field, respectively.

order contamination ($\lambda/2$, $\lambda/3$, etc.). We performed large angle diffraction experiments in a horizontal field of 2.6 T and field reversal experiments in a vertical magnetic field up to 7.5 T applied along the [1$\bar{1}$0] direction as shown in Fig. 1. PNR experiments were performed in a vertical field up to 7.5 T, and the polarization of the incident neutron beam was 96%.[12]

The sample was aligned with the [1$\bar{1}$0] crystallographic orientation perpendicular to the scattering plane (see Fig. 1). With diffraction, we were then able to measure reflections of the type (HHL). The intensity of the different reflections is the sum of a nuclear term, resulting from the chemical order, and a magnetic term, resulting from the ordered magnetic moments. For unpolarized neutrons, the measured intensity I can be written as $I=|F_{nuc}|^2+|F_{mag}|^2$. The nuclear structure factor F_{nuc} describes the scattered amplitude from all atoms as function of the scattering vector $q=4\pi\sin(\theta)/\lambda$. By ignoring the Debye-Waller factor, the structure factor can be obtained by summing over the contributions of all atoms in the unit cell:

$$|F_{nuc}|^2 = \left| \sum_k b_k \exp(i\mathbf{q}\cdot\mathbf{r}_k) \right|^2, \tag{1}$$

with b_k being the nuclear scattering length of an atom at the position $\mathbf{r}_k$. The scattered magnetic intensity can be written as[13]

$$|F_{mag}|^2 = \frac{g_n^2 r_0^2}{16} \sum_{k,l} \{f_k f_l (\boldsymbol{\mu}_k\cdot\boldsymbol{\mu}_l - (\hat{\mathbf{q}}\cdot\boldsymbol{\mu}_k)(\hat{\mathbf{q}}\cdot\boldsymbol{\mu}_l)) \times \exp[i\mathbf{q}\cdot(\mathbf{r}_k-\mathbf{r}_l)]\}, \tag{2}$$

with the neutron g factor[14] $g_n=-3.826$, the classical electron radius $r_0=\mu_0 e^2/4\pi m_e$, the q-dependent magnetic form factor f_k, the magnetic moment in Bohr magnetons $\boldsymbol{\mu}_k$ of an atom at the position $\mathbf{r}_k$, and the unit vector $\hat{\mathbf{q}}$ along **q**.

TABLE I. Accessible Bragg reflections and their structure factors calculated using the coherent neutron scattering lengths, b_{RE} and b_{Fe}, and Eq. (1).

Reflection	$\lvert F_{nuc}\rvert^2$	$\lvert F_{nuc}\rvert^2$ (fm^2)
(220)	$(2b_{RE})^2$	609.6
(004)	$4(b_{RE}-2b_{Fe})^2$	171.9
(113)	$(\sqrt{2}b_{RE}+2b_{Fe})^2$	1321.9
(111)	$(\sqrt{2}b_{RE}-2b_{Fe})^2$	2.1
(222)	$(4b_{Fe})^2$	1428.8

As can be easily seen from Eq. (2), the magnetic contribution to the scattered intensity is a maximum if $\mathbf{q}\perp\boldsymbol{\mu}$, whereas the contribution is zero for $\mathbf{q}\parallel\boldsymbol{\mu}$. Ignoring the angular dependence the magnetic scattering length $b_{mag,k}$ of an atom at the position $\mathbf{r}_k$ is proportional to the magnetic moment $\boldsymbol{\mu}_k$ and the form factor $f(q)$:

$$b_{mag} = \frac{\mu_0 e^2 g_n}{16\pi m_e}\mu_k f(q) = 2.695\ \text{fm}\times\mu_k\times f(q). \tag{3}$$

By measuring the intensity of Bragg peaks associated with different crystallographic orientations, neutron diffraction is capable of determining the direction of the sample's magnetization. The accessible Bragg reflections for the Laves phase in the (HHL) scattering plane are listed in Table I together with the structure factors for the nuclear part of the reflected intensity. The (220) reflection depends only on the properties of the rare earths, the (222) reflection only on the Fe properties, whereas the other reflections contain contributions from both the rare earths and the Fe atoms. For the calculations listed in Table I, we used $b_{Fe}=9.45$ fm and $b_{RE}=12.345$ fm for the average of Dy and Er.[15]

III. EXPERIMENTAL RESULTS

In order to check the dependence of different Bragg reflections on the orientation of the magnetization with respect to **q**, we applied a horizontal field $\mu_0 H_{ext}=2.6$ T parallel and perpendicular to the **q** of the measured Bragg reflections. We did these measurements at 290 K to overcome the magnetic anisotropies and saturate the sample. When the magnetization is parallel to the field direction, only the nuclear intensity $|F_{nuc}|^2$ is measured, whereas the maximum magnetic contribution is measured for $\mathbf{H}_{ext}\perp q$. Table II shows a comparison of the experimentally determined and calculated intensity ratios at 290 K assuming $\mu_{Fe}=1.4$ and $\mu_{RE}=5.91$ at 290 K, and $\mu_{Fe}=1.6$ and $\mu_{RE}=9.5$ at 4 K,[1,16] with the magnetic moment given in units of μ_B per atom.

As can be seen from Tables I and II, the (111), (220), and (004) Bragg reflections have large magnetic components to their intensity. The agreement between theory and experiment in the ratios of the intensity is poor, possibly because the magnetic field was not large enough to align all the moments parallel to the applied field, possibly due to errors in the assumed magnitude of the magnetic moments, and, finally, possibly because the magnetic and nuclear scatterings

TABLE II. Comparison of the calculated and experimentally determined ratios of the maximum intensity (magnetic plus nuclear) to the nuclear intensity for various Bragg reflections at 290 K.

Reflection	$\lvert F_{max}/F_{nuc}\rvert^2$ (Calc., 4 K)	$\lvert F_{max}/F_{nuc}\rvert^2$ (Calc., 290 K)	$\lvert F_{max}/F_{nuc}\rvert^2$ (Expt., 290 K)
(220)	4.4	2.3	1.5
(004)	17.4	8.6	6.3
(113)	1.5	1.1	1.5
(111)	869.7	390.7	3.6
(222)	1.1	1.1	1.0

could be altered by multiple scattering. Nevertheless, there is a qualitative agreement with the theory showing which reflections have a large effect, and we shall only need the changes in the magnetic intensity qualitatively in the analysis of the data.

The magnetic contributions can be used to follow the changes in the magnetization when an applied field is reversed. The sample was aligned in a vertical field cryomagnet and then cooled to 4 K in a magnetic field of −7.5 T. The field was then increased, keeping the temperature at 4 K and measuring the scattered intensity for the (111), (004), (220), and (113) reflections. The measured intensities were normalized to the observed intensities in a field of −7.5 T and are shown in Fig. 2. The intensities in zero applied field are virtually unchanged, showing that the structure at remanence and at saturation are the same. On increasing the magnetic field, there is a clear decrease in the intensity of about 50% in the (220) and (111) Bragg reflections at about 2.5 T. On further increasing the field, the intensity recovers and is the same at 7.5 T as at −7.5 T. This result can be interpreted as a rotation of the magnetization from the $[1\bar{1}0]$ direction toward the [220] and [111] directions. In more detail, the intensity of the (004) reflection decreases by only about 10% at 2.5 T, and we can interpret this and the behavior of the (220) and (111) reflections as consistent with the average magnetization at 2.5 T being horizontal and about 20° away from the [110] growth direction. This direction corresponds to the [221] direction that was found to be the easy direction for thin $ErFe_2$ films[9] at 4 K.

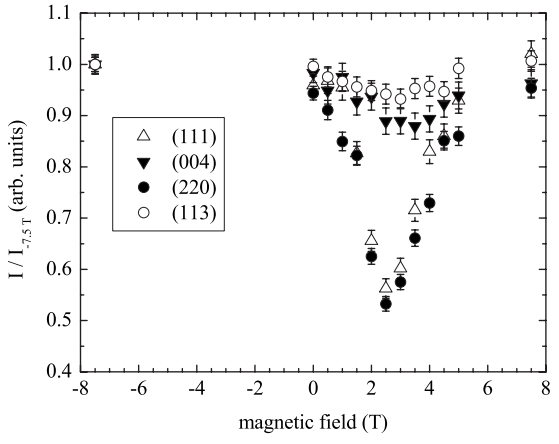

FIG. 2. Bragg peak intensity for the (111), (004), (220), and (113) reflections measured at 4 K as a function of increasing magnetic field applied parallel to the $[1\bar{1}0]$ direction. Prior to the measurements, the sample was saturated in a field of −7.5 T.

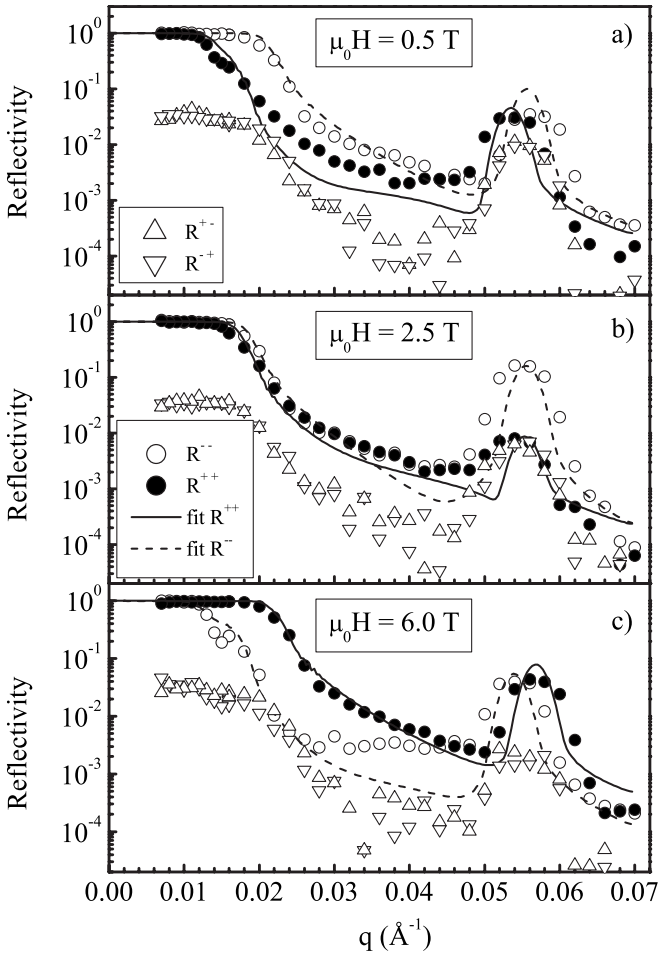

FIG. 3. Neutron reflectivities R^{++} (solid circles), R^{--} (open circles), R^{+-} (up triangles), and R^{-+} (down triangles) along with the fits for R^{++} (solid line) and R^{--} (dashed line), measured at 4 K in magnetic fields of (a) 0.5 T, (b) 2.5 T, and (c) 6 T. Prior to the measurements, the sample was saturated in a field of −7.5 T along the $[1\bar{1}0]$ direction.

Further information about the magnetization could be found from PNR. The sample was aligned in the same geometry as illustrated in Fig. 1 and the reflectivity measured for wave vectors from 0 to 0.07 $Å^{-1}$. Four different neutron spin cross sections were measured at a temperature of 4 K corresponding to R^{++}, R^{--}, R^{+-}, and R^{-+}, where the first superscript refers to the incident neutron spin state and the second superscript refers to the scattered neutron spin state. A selection of the results obtained is shown in Fig. 3 as the strength of the applied field is varied. The displayed spin-flip reflectivities represent as-measured data without a correction based on the measured flipping ratio. Prior to the measurements, the sample was saturated in a field of −7.5 T along the $[1\bar{1}0]$ direction.

The non-spin-flip reflectivity can be described with the Fermi pseudopotential (nuclear interaction) and a Zeeman

term (magnetic interaction).[17–19] For the neutrons with spin parallel to the external field (spin-up neutrons), the magnetic potential adds to the nuclear one, whereas for the spin-down neutrons, the magnetic potential is subtracted from the nuclear potential. Therefore, the critical edge for spin-down neutrons is different from the one for spin-up neutrons as can be seen in Fig. 3, where the critical edge at small wave vectors is different for R^{++} and R^{--}, and changes sign between 0.5 and 6 T. However, both cross sections are the same for 2.5 T when the net magnetization along the field direction was very small. A spin-flip intensity R^{+-} or R^{-+} occurs if the sample has an in-plane magnetization component perpendicular to the spin of the neutrons. In our setup shown in Fig. 1, magnetization components along [001] would cause spin-flip scattering. The complete theoretical description of all four neutron cross sections requires a matrix formalism.[17–19]

The critical edge of the reflectivity curves near $q=0$ gives information about the average magnetizations of the $ErFe_2$ and $DyFe_2$ layers, while the position of the superlattice peak at 0.055 $Å^{-1}$ gives information largely about the layer thicknesses. The small differences in the position of the peak for R^{++} and R^{--} arise because the spin-up and spin-down neutrons have slightly different refractive indices in the superlattice, giving a small dynamical scattering correction to the peak position. The magnetic intensity of this peak depends on the difference of the net magnetization in the two layers of the superlattice. There is little difference in this for the magnetic fields of 0.5 and 7.5 T, but for 2.5 T, the difference is large and the intensity is largest for R^{++}, while it is largest for R^{--} for a field of 4 T. The reflectivity curves shown in Fig. 3 were fitted in detail using the Parratt formalism[20] and by assuming that each type of layer had the same magnetization profile throughout the superlattice. Our conclusions from this analysis depend sensitively only on the reflectivity near $q=0$ and near the superlattice peak. Discrepancies elsewhere result largely from errors introduced by structural effects at the surface of the superlattice and the interface to the buffer layer, and are not significant to our results.

The as-measured spin-flip intensities are displayed in Fig. 3 as triangles. The flipping ratio of our setup was about 30, as can be determined from the data points in the low-q region, where no spin-flip intensity is present. During the magnetization reversal, no increase in the spin-flip intensity can be observed. This supports the interpretation of the diffraction experiments that the sample's magnetization is reversed via a rotation mainly through the out-of-plane direction. Otherwise, a large spin-flip signal should be observable close to the coercive field as has been observed, e.g., in the exchange-bias system Co/CoO.[21,22] Simulations (not shown here) confirm that a deviation of 70° of the layer magnetization from the [001] spin-flip axis does not give a detectable amount of spin-flip intensity, i.e., the expected spin-flip contribution would be within the error limits of the measurement. The reason for the small spin-flip contribution is the angular dependence of the spin-flip intensity, which is proportional to $\cos^2 \alpha$, with α being the angle between the spin-flip axis [001] and the magnetization.[22,23] Therefore, small perpendicular in-plane magnetization components are hard to detect with PNR.

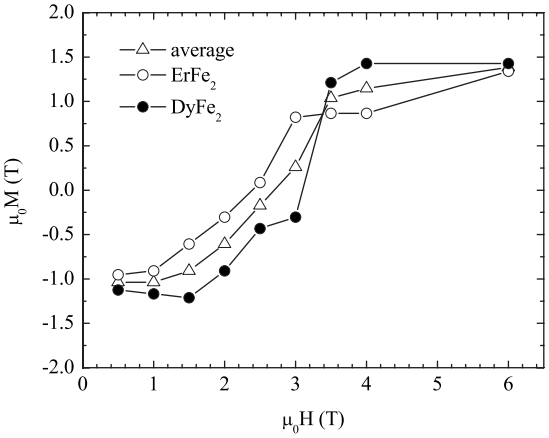

FIG. 4. Magnetization in the $[1\bar{1}0]$ direction for the $DyFe_2$ layers (solid circles) and the $ErFe_2$ layers (open circles), measured at 4 K. The average magnetization is displayed as triangles. Prior to the measurements, the sample was saturated in a field of −7.5 T along the $[1\bar{1}0]$ direction and then the field increased.

From the fit data, we can infer the magnetization component of the $DyFe_2$ and $ErFe_2$ layers parallel to the external magnetic field independently. The values are shown in Fig. 4, with the closed circles representing the magnetization component of the $DyFe_2$ layers and the open circles the magnetization component of the $ErFe_2$ layers. The average value that would be measured by classical magnetometry is displayed as triangles. The coercive field of 2.5 T nicely corresponds to the minimum in the (220) peak intensity in Fig. 2. The $DyFe_2$ magnetization rotates faster through the [221] direction than the $ErFe_2$ magnetization because it is a magnetic hard axis for $DyFe_2$.

IV. CONCLUSION

We have studied using both reflectivity and large angle neutron scattering techniques a superlattice with equal thickness layers of $ErFe_2$ and $DyFe_2$ and with a growth axis parallel to the cubic [110] direction. It was magnetized along the perpendicular $[1\bar{1}0]$ direction, and the field then reversed so that the magnetization reverses through the [221] direction. The [221] direction is the easy axis for $ErFe_2$ thin films,[9] but is not an easy axis for bulk $ErFe_2$, which has the [111] direction as the easy axis. The difference in the anisotropy arises because the superlattice is strained when grown and the strain makes a very significant contribution to the anisotropy of these almost cubic materials. Furthermore, the strong Fe-Fe exchange coupling between the layers has resulted in the magnetization of the $DyFe_2$ closely but not exactly following the $ErFe_2$ magnetization. This [221] direction is not an easy magnetic direction for the $DyFe_2$. An easy direction perpendicular to the growth direction[9] was determined from experiments on single $DyFe_2$ films. Nevertheless, our results show that the anisotropy of the magnetic moments of the $ErFe_2$ is considerably stronger than the anisotropy of the magnetic moments for the $DyFe_2$. This illustrates the unexpected nature of the anisotropy in this sample with two magnetically hard materials.

*helmut.fritzsche@nrc.gc.ca

[1] A. E. Clark, in *Handbook on the Physics and Chemistry of Rare Earths*, edited by K. A. Gscheidner and L. Eyring (North-Holland, Amsterdam, 1979).
[2] A. E. Clark, in *Ferromagnetic Materials*, edited by E. P. Wohlfarth (North-Holland, Amsterdam, 1980).
[3] J. Ilarraz and A. Del Moral, Phys. Status Solidi A **57**, 89 (1980).
[4] M. Sawicki, G. J. Bowden, P. A. J. de Groot, B. D. Rainford, J. M. L. Beaujour, R. C. C. Ward, and M. R. Wells, Phys. Rev. B **62**, 5817 (2000).
[5] K. Dumesnil, M. Dutheil, C. Dufour, and P. Mangin, Phys. Rev. B **62**, 1136 (2000).
[6] S. N. Gordeev, J. M. L. Beaujour, G. J. Bowden, P. A. J. de Groot, B. D. Rainford, R. C. C. Ward, and M. R. Wells, J. Appl. Phys. **89**, 6828 (2001).
[7] M. J. Bentall, R. A. Cowley, W. J. L. Buyers, Z. Tun, W. Lohstroh, R. C. C. Ward, and M. R. Wells, J. Phys.: Condens. Matter **15**, 4301 (2003).
[8] M. R. Fitzsimmons, S. Park, K Dumesnil, C. Dufour, R. Pynn, J. A. Borchers, J. J. Rhyne, and P. Mangin, Phys. Rev. B **73**, 134413 (2006).
[9] A. Mougin, C. Dufour, K. Dumesnil, and Ph. Mangin, Phys. Rev. B **62**, 9517 (2000).
[10] A. Mougin, C. Dufour, K. Dumesnil, N. Maloufi, P. Mangin, and G. Patrat, Phys. Rev. B **59**, 5950 (1999).
[11] J. Bergsma and C. van Dijk, Nucl. Instrum. Methods **51**, 121 (1967).
[12] H. Fritzsche, Rev. Sci. Instrum. **76**, 115104 (2005).
[13] G. L. Squires, *Introduction to the Theory of Thermal Neutron Scattering* (Dover, Mineola, 1996).
[14] http://physics.nist.gov/cuu/index.html
[15] V. F. Sears, Neutron News **3**, 26 (1992).
[16] J. J. Rhyne, J. Magn. Magn. Mater. **70**, 88 (1987).
[17] G. P. Felcher, R. O. Hilleke, R. K. Crawford, J. Haumann, R. Kleb, and G. Ostrowski, Rev. Sci. Instrum. **58**, 609 (1987).
[18] S. J. Blundell and J. A. C. Bland, Phys. Rev. B **46**, 3391 (1992).
[19] F. Radu, V. Leiner, M. Wolff, V. K. Ignatovich, and H. Zabel, Phys. Rev. B **71**, 214423 (2005).
[20] L. G. Parratt, Phys. Rev. **95**, 359 (1954).
[21] M. Gierlings, M. J. Prandolini, H. Fritzsche, M. Gruyters, and D. Riegel, Phys. Rev. B **65**, 092407 (2002).
[22] W. T. Lee, S. G. E. te Velthuis, G. P. Felcher, F. Klose, T. Gredig, and E. D. Dahlberg, Phys. Rev. B **65**, 224417 (2002).
[23] N. K. Pleshanov, Physica B **269**, 79 (1999).